PCCP

Accepted Manuscript

ROYAL SOCIETY OF CHEMISTRY

www.rsc.org/pccp

Journal Name

RSCPublishing

ARTICLE

Composite cathode based on scandium doped titanate with enhanced electrocatalytic activity towards direct carbon dioxide electrolysis

Cite this: DOI: 10.1039/x0xx00000x

Liming Yang,[a] Kui Xie,[a,b] * Lan Wu,[a] Qingqing Qin,[a] Jun Zhang,[a] Yong Zhang,[a] Ting Xie, [a] Yucheng Wu[a,b] *

Received 00th January 2012,
Accepted 00th January 2012

DOI: 10.1039/x0xx00000x

www.rsc.org/

Composite cathode based on redox-stable $La_{0.2}Sr_{0.8}TiO_{3+\delta}$ (LSTO) can perform direct carbon dioxide electrolysis; however, the insufficient electro-catalytic activity limits the electrode performances and current efficiencies. In this work, catalytic-active scandium is doped into LSTO to enhance the electro-catalytic activity for CO_2 electrolysis. The structures, electronic conductivities and ionic conductivities of $La_{0.2}Sr_{0.8}Ti_{1-x}Sc_xO$ ($LSTS_xO$) (x=0, 0.05, 0.1, 0.15 and 0.2) are systematically studied and further correlated to electrode performances. The ionic conductivities of single-phase $LSTS_xO$ (x=0, 0.05, 0.1 and 0.15) remarkably improve *versus* the scandium doping contents though the electrical conductivities gradually change in an adverse trend. Electrochemical measurements demonstrate promising electrode polarisations of $LSTS_xO$ electrodes and increasing scandium doping contents accordingly improves electrode performances. The Faradic efficiencies of carbon dioxide electrolysis are enhanced by 20% with $LSTS_{0.15}O$ in contrast to bare LSTO electrode in a solid oxide electrolyser at 800 ºC.

Introduction

Solid oxide electrolysers have shown enormous advantages of efficient electrochemical conversion of carbon dioxide into fuels using renewable electrical energy.[1-3] The oxide-ion-conducting solid oxide electrolysers can directly electrolyze CO_2 into CO fuel and pure O_2 under applied voltages. At cathode, CO_2 molecules are electrochemically reduced into CO and O^{2-} which transports through electrolyte membrane to anode and transforms to O_2 gas.

Conventional Ni-YSZ has been preferentially utilized as cathode for high-temperature carbon dioxide electrolysis in oxide-ion-conducting solid oxide electrolysers.[4-7] However, the inherent redox instability of Ni-YSZ is always the limitation and a significant concentration of reducing gas is needed to flow over the Ni cermets to avoid oxidation of Ni to NiO which leads to the loss of electrical conductivity and electrode performance degradation. Irvine and Yang et al reported that Ni-YSZ cathode can be oxidized at high temperature for direct carbon dioxide electrolysis that causes considerable electrode degradation.[8] We have also observed that the mixture of CO_2/H_2O can quickly oxidize Ni metal into amorphous phase composed of NiO and $Ni(OH)_2$.[9]

In contrast to Ni-YSZ, the perovskite-type $La_xSr_{1-x}Cr_yMn_{1-y}O_{3-\delta}$ (LSCM) has been proved to be an active and redox-stable material which has attracted giant attentions in the field of high-temperature solid oxide cells.[10-14] Irvine et al have recently proved the efficient

electrolysis of CO_2 based on a ceramic LSCM cathode without using a flow of CO, and it has been found that CO is steadily produced from cathode. This means that LSCM can be used as the efficient cathode material of solid oxide electrolyser because it exhibits comparable cathode performances compared to traditional Ni-YSZ cermet.[15] The direct CO_2 electrolysis with LSCM cathode has also been achieved in our previous work without reducing gas over the electrode.[16] Promising electrode performances and current efficiencies have been demonstrated; however, the p-type conduction mechanism of LSCM is not ideally adapted to reducing potential which causes to a large electrode polarization resistance and low current efficiency under high electrolysis voltages.[17-19]

The perovskite titanate $La_xSr_{1-x}TiO_{3+\delta}$ (LSTO) is an active and redox-stable material with n-type conduction mechanism upon reduction, which leads to the material receiving a great attention in the field of high-temperature solid oxide fuel cells.[20-24] Irvine et al have reported that the perovskite LSTO composite anode is well adapted to the reducing atmosphere.[25] The metallic-type conduction mechanism of LSTO upon reduction would well fit the strongly reducing condition and result in better electrode performances. Composite cathode based on $La_{0.2}Sr_{0.8}TiO_3$ has been confirmed to be well adapted to the reducing condition for steam electrolysis in electrolyzers.[26] We have performed direct steam electrolysis to produce hydrogen in an oxide-ion-conducting solid oxide electrolyser based on LSTO cathode. It is found that the current efficiency reaches 30% and 58% at 1.6 and 2.0 V for steam electrolysis at 800 ºC, respectively. The insufficient electro-catalytic activity of LSTO ceramic still limits the electrode performance and current efficiencies for high temperature steam electrolysis.[27,28]

Scandium oxide has been commonly considered as an electrocatalyst and utilized to enhance electrocatalytic activity of composite electrodes.[25,29] Due to its unique catalytic property, scandium element has been widely doped into perovskite electrode materials to improve the electrode performance. For example, the doping of scandium in the B-site of perovskite $(La,Sr)MnO_3$ increases oxygen vacancy concentration and decreases oxygen migration energy as reported by Zhao.[31,32] Cheng et al reported that the anode based on scandium-doped manganate composite electrode exhibits 1.4 $W \cdot cm^{-2}$ with hydrogen fuel at 800 ºC, which can be ascribed to the increased oxygen vacancies and improved electrode activity in manganate. Moreover, only minor amount of scandium substitution is already beneficial to the improvement of electrode performance.[33] The generation of oxide-ion vacancies is expected to improve ionic conductivity and lower electrode polarisation which is beneficial to the improvement in electrode performance. Oxide vacancies are not only expected to increase ionic conductivity, but also to exhibit chemical adsorption behavior by accommodating molecules.[34-36] We have reported the remarkable chemical adsorption of CO_2 on doped titanate with sufficient oxygen vacancies and the onset temperature of strong chemical desorption is extended to as high as approximately 800 °C of the common operation temperature for solid oxide carbon dioxide electrolysers. The oxygen vacancies accommodate and activate CO_2 molecules in the form of strong bonding between the oxide ions in CO_2 and the nearest cations in titanate cathode.[24]

In this work, the catalytic-active scandium is doped into the B-site of redox-stable $La_{0.2}Sr_{0.8}TiO_{3+\delta}$ in order to improve the electrocatalytic activity for high temperature carbon dioxide electrolysis. The structure, electronic conductivity and ionic conductivity of $LSTS_xO$ (x=0, 0.05, 0.1, 0.15) are systematically studied and closely correlated to electrochemical performances. The CO_2 electrolysis is investigated with scandium-doped LSTO cathode in an oxide-ion-conducting solid oxide electrolyser at 800 ºC.

Experimental

All the powders used in this work were bought from SINOHARM Chemical Reagent Co. Ltd (China) unless special instructions. The $La_{0.2}Sr_{0.8}Ti_{1-x}Sc_xO_3$ (x=0, LSTO; x=0.05, $LSTS_{0.05}O$; x=0.1, $LSTS_{0.1}O$; x=0.15, $LSTS_{0.15}O$, x=0.2, $LSTS_{0.2}O$) powders were synthesized by a traditional solid-state reaction method.[37] Stoichiometric amount of powers of La_2O_3, $SrCO_3$, TiO_2 and Sc_2O_3 were mixed in acetone and ball-milled with zirconia balls for 10 minutes. The dried mixture was pressed into pellets (pressure=4 Mpa) at room temperature and fired at 1400 °C (3 °C·min^{-1}) for 10 h in air. These pellets were then grinded into yellowish powders. Then part of the $LSTS_xO$ (x= 0, 0.05, 0.1, 0.15) powders were treated in 5%H_2/Ar at 1400 °C (3 °C·min^{-1}) for 10 h to reduce the samples followed by XRD tests. The $Ce_{0.8}Sm_{0.2}O_{2-\delta}$ (SDC) powders were prepared by a combustion method with proper amounts of Sm_2O_3 and $Ce(NO_3)_3{\cdot}6H_2O$ precursors and then treated at 800 °C (3 °C·min^{-1}) for 3 h in air. The $(La_{0.8}Sr_{0.2})_{0.95}MnO_{3-\delta}$ (LSM) powders were prepared by a combustion method with La_2O_3, $SrCO_3$ and $C_4H_6Mn{\cdot}4H_2O$ with the heat treatment at 1100 °C (3 °C·min^{-1}) for 3 h in air.[38] The phase structures of $LSTS_xO$ (x=0, 0.05, 0.1, 0.15, 0.2), LSM and SDC powders were acquired by X-ray Diffraction (XRD, 2θ=20-80º, D/MAX2500V, Rigaku Corporation, Japan). High-resolution Transmission Electron Microscopy analysis (HRTEM) (JEM-2100F, JEOL, Japan) with selected area diffraction was performed to observe the structure changes of oxidized and reduced samples. X-ray Photoelectron Spectroscopy (XPS, ESCALAB250, USA) was performed on a Thermo ESCALAB 250 using monochromatized Al Ka to analyze the surface of oxidized and reduced LSTSO powders. Thermogravimetry Analysis (TGA, STA449F3, Germany) was used to analyse the oxygen nonstoichiometry of the reduced LSTO and $LSTS_{0.15}O$ samples. The microstructure of the electrolyzer was observed using Scanning Electron Microscopy (SEM, SU8020, Japan).

About 2.0 g $LSTS_xO$ (x=0, 0.05, 0.1 and 0.15) powders were pressed into bars at the pressure of 8 MPa and then sintered at 1400 ºC for 10 h in air, respectively. The prepared bars were reduced at 1400 ºC for 10 h in 5%H_2/Ar for conductivity tests. The conductivity tests were performed in a reducing atmosphere (5%H_2/Ar) using DC four-terminal method with temperature ranging from 20 to 800 ºC to investigate the relationship between conductivity and temperature. The conductivity was recorded *versus* temperature using an online system at a step 0.5 ºC. Similarly, about 2.0 g $LSTS_xO$ (x=0, 0.05, 0.1 and 0.15) powders were pressed into pellets, sintered and then reduced at 1400 ºC in 5%H_2/Ar for ionic conductivity tests. The ionic conductivity was tested in 5%H_2/Ar from 400 to 800 ºC using electron-blocking electrode method.[24] The conductivity was recorded with an online multi-meter (Keithley 2000, Digital Multimeter, Keithley Instruments Inc., USA).

A 1-mm-thick YSZ electrolyte pellet was made by pressing YSZ powders into a green disk with a diameter of 15 mm, followed with sintering at 1550 ºC for 20 h in air. The two surfaces of the obtained YSZ electrolyte pellets were mechanically polished and then ultrasonically cleaned in distilled water. The $LSTS_xO$-SDC (x=0, 0.05, 0.1 and 0.15) composite electrode slurries were prepared by milling the SDC powder with $LSTS_xO$ powder at a weight ratio of 35:65 in alpha terpineol with proper amounts of cellulose, respectively. To prepare symmetric cells with the configurations of $LSTS_xO$-SDC/YSZ/$LSTS_xO$-SDC (x=0, 0.05, 0.1 and 0.15), the electrode slurries were coated onto the two surfaces of electrolyte in symmetric positions in area of 1 cm^2 and then treated at 1100 ºC (3 °C·min^{-1}) for 3 h in air. Silver paste (SS-8060, Xinluyi, Shanghai, China) was printed on both surfaces of the electrodes to collect current. The external circuit was made with silver wire (about 0.4

mm in diameter), which was connected to current collectors using conductive adhesive (DAD87, Shanghai Research Institute for Synthetic Resins, Shanghai, China) followed by treating at 550 ºC (3 °C·min^{-1}) for 30 min.[38] The AC impedance of symmetric cells was tested in different hydrogen pressure and different carbon monoxide pressure at 800 ºC using the electrochemical workstation (IM6, Zahner, Germany) with a frequency ranging from 1 M Hz to 0.1 Hz at the open circuit voltage (OCV), respectively. Different hydrogen pressure was controlled using a mass flow meter (D08-3F, Sevenstar, Beijing, China) at a speed of 20 ml·min^{-1} to mix H_2 and N_2. Different carbon monoxide pressure was also controlled by mixing 5%CO/Ar and CO_2. The electrode polarization resistance was calculated by modeling the spectra using Zview software.[18] The solid oxide electrolysers were made with LSM-SDC anode and LSTO-SDC or $LSTS_{0.15}O$-SDC cathode in the same way as described above. The electrolysers were sealed on a home-made testing jig using ceramic paste (JD-767, Jiudian, Dongguan, China) for electrochemical measurements including AC impedance and current-voltage (I-V curve). The carbon dioxide electrolysis was performed using an electrochemical station at different applied voltages (1.0, 1.2, 1.4, 1.6, 1.8 and 2.0V) with CO_2 fed into cathode at 800 ºC, respectively. The concentration of carbon monoxide in output gas from cathode was checked using an online gas chromatograph (GC9790II, Fuli, Zhejiang, China).

Results and discussion

Fig. 1 (a) shows the XRD patterns of the $La_{0.2}Sr_{0.8}Ti_{1-x}Sc_xO_{3+\delta}$ (x=0, 0.05, 0.1, 0.15 and 0.2) samples. Single-phase perovskite structure can be observed with the scandium doping level below 15%, confirming the successful partial replacement of Ti^{4+} by Sc^{3+} in B-site. A small peak of scandia appears when the scandium doping level exceeds 15%, which shows the solubility limit of scandia in the titanate. Table 1 shows parameters of oxidized $LSTS_xO_3$ (x=0, 0.05, 0.1 and 0.15). As shown in Table 1, the structures of the $LSTS_xO_3$ (x=0, 0.05, 0.1 and 0.15) are cubic with Pm-3m space group. As shown in Fig. 1 (c), the cell parameters for oxidized $La_{0.2}Sr_{0.8}Ti_{1-x}Sc_xO_3$ (x=0, 0.05, 0.1 and 0.15) are 3.9047(4), 3.9068(3), 3.9095(5) and 3.9122(6) Å, respectively. The lattice parameters linearly increase *versus* the Sc doping contents because the Sc^{3+} (0.885 Å) with larger ionic radii than Ti^{4+} (0.605 Å), which is well consistent with Vegard's law. With the rise of Sc content, the cell parameters gradually increase and vary linearly, which is due to the larger ionic radii of Sc^{3+} than Ti^{4+} with the same coordination numbers.[21,39,40] Fig. 1 (b) shows the XRD patterns of the reduced $LSTS_xO$ (x=0, 0.05, 0.1 and 0.15) treated in 5%H_2/Ar at 1400 ºC for 10 h, and also display pure phase. No phase change is observed for $LSTS_xO$ (x=0, 0.05, 0.1 and 0.15) even after the high-temperature reduction in an extremely reducing atmosphere, which is a powerful evidence of the redox stability of titanate ceramics. As shown in Table 2, the structures of the reduced $LSTS_xO_3$ (x=0, 0.05, 0.1 and 0.15) are also cubic with Pm-3m space group. Slight increases are observed on cell parameter, which is due to the presences of Ti^{3+} in reduced samples.[26] As shown in Fig. 1(d), the cell parameters for reduced $La_{0.2}Sr_{0.8}Ti_{1-x}Sc_xO_3$ (x=0, 0.05, 0.1 and 0.15) are 3.9082(4), 3.9090(1), 3.9112(3) and 3.9131(9) Å, respectively. Similarly, the lattice parameters increase linearly with the rise of Sc content which well corresponds to the Vegard's law.

Fig. 2 (a1) and (a2) show the XRD Rietveld refinement patterns of the oxidized and reduced LSTO powders, respectively. The site position data of La and Sr in $La_{0.2}Sr_{0.8}Ti_{1-x}Sc_xO_{3+\delta}$ samples are same and give x, y, z and B values of 0, 0, 0 and 0.7419, respectively. The site position data of Ti and Sc in $LSTS_xO$ samples are same and give x, y, z and B values of 0.5, 0.5, 0.5 and 0.3575, respectively. The site position data of O in $LSTS_xO$ samples give x, y, z and B values of 0, 0.5, 0.5 and 0, respectively. The refinements of the oxidized and

reduced LSTO samples give wRp and Rp, chi^2 values of 9.13%, 6.8% and 1.657 as well as 6.41%, 5.03% and 0.9971, respectively, suggesting a close fit to the experimental data. According to the experimental data and calculated results, it is demonstrated that the phase structure of both oxidized and reduced samples can be determined as perovskite structure with space group of Pm-3m.[20] The cell parameter of the oxidized LSTO is 3.9047(4) Å which is slightly smaller than the 3.9082(4) Å for the reduced LSTO. This is due to that titanium is mainly Ti^{4+} (0.605 Å) in the oxidized LSTO while a part of Ti^{4+} transform into Ti^{3+} (0.670 Å) in the reduced LSTO, which is expected to lead to the cell parameter expansion. However, no phase change is observed for the LSTO even after the high-temperature reduction. As shown in Fig. 2 (b1) and (b2) the refinements of the oxidized and reduced $LSTS_{0.15}O$ samples give wRp, Rp, chi^2 values of 9.5% and 7.14% and 1.562 as well as 10.01%, 6.8% and 1.778, respectively, which reveals the successful partial replacement of Ti by Sc in B-site of titanate. The cell parameter of the oxidized $LSTS_{0.15}O$ is 3.9122(6) Å slightly larger than that of oxidized LSTO, which may relate to the larger ionic radii of Sc^{3+} (0.885 Å) than Ti^{4+} with the same coordination numbers. Similarly, the small change of crystal cell parameters between the oxidized and reduced $LSTS_{0.15}O$ is also because of the presence of Ti^{3+} in the reduced sample. As shown in Fig. 3 (a1) and (a2), TEM analysis of the oxidized and reduced LSTO has revealed lattice spacing of 2.764 Å (110) and 2.773 Å (110), respectively, which is consistent with the lattice parameter showed by the XRD analysis in Fig. 3 (b1) and (b2). The corresponding lattice spacing of the oxidized scandium-doped sample has increased from 2.846 Å (110) to 3.042 Å (110) for the reduced scandium-doped sample in Fig. 3 (b1) and (b2), further demonstrating the lattice expansion of the reduced sample as determined by the XRD analysis.

To confirm the change of elemental valence in samples, XPS analysis is performed to test the oxidized and reduced $LSTS_{0.15}O$ samples. All the XPS spectroscopies are fitted with a Shirley-type background subtraction method. The background-functions for different elements spectroscopies are fitted with 20% Lorenz and 80% Gaussian. As shown in Fig. 4 (a1), only Ti^{4+} is observed in the oxidized $LSTS_{0.15}O$ sample; however, part of the Ti^{4+} is chemically reduced to Ti^{3+} by treating the sample in a reducing atmosphere. In Fig. 4 (b1), the Ti^{4+} (2p3/2), Ti^{3+} (2p3/2), Ti^{3+} (2p1/2) and Ti^{4+} (2p1/2) peaks are observed at 458.3, 458.9, 463.4 and 464.3 eV in reduced $LSTS_{0.15}O$ sample, respectively.[41-43] As shown in Fig. 4 (a2) and (b2), only Sc^{3+} is observed in oxidized and reduced samples. The XPS data demonstrates that Sc has a fixed chemical valance state in oxidized or reduced sample; the only change is transformation of higher-energy Sc^{3+} into lower energy state.[44]

In order to analyse the oxygen nonstoichiometry, TGA tests is performed for reduced LSTO and $LSTS_{0.15}O$ from room temperature to 1000 ºC (10 ºC·min^{-1}) in air as shown in Fig. 5. The reduced LSTO gains the rapid weight increase of 0.78 wt% from 500 to 600 ºC and varies in a very small range from 700 to 1000 ºC, which suggests the sufficient oxidation of reduced LSTO powders. The reduced LSTO demonstrates a chemical formula of $La_{0.2}Sr_{0.8}TiO_{3.005}$ in contrast to the oxidized LSTO with a chemical formula of $La_{0.2}Sr_{0.8}TiO_{3.100}$, which indicates that 18% of Ti^{4+} has been transformed to Ti^{3+} in reduced LSTO sample. Nevertheless, the transformation of Ti^{4+} to Ti^{3+} is not accompanied by the creation of oxygen vacancy with the decrease of the coordination number of Ti but with the loss of excess interstitial oxygen.[24] In contrast, the reduced $LSTS_{0.15}O$ with weight increase of 0.66 wt% indicates that the concentration of Ti^{3+} drops to 15%, which is expected to lead to the decrease of electrical conductivity. The reduced $LSTS_{0.15}O$ determines a chemical formula of $La_{0.2}Sr_{0.8}TiO_{2.947}$ accompanied by

the 0.053 mol oxygen loss per chemical formula unit in contrast to the oxidized $LSTS_{0.15}O$ with chemical formula of $La_{0.2}Sr_{0.8}Ti_{0.85}Sc_{0.15}O_{3.025}$. The doping of La in the A-site produces oxygen interstitial and the reduction of sample lowers the amount of oxygen interstitials without changing the coordination number of Ti in perovskite. In contrast, the doping of Sc in LSTO further drops the amount of oxygen that is beneficial to the enhancement of ionic conductivity.

Fig.6 shows the dependence of conductivity and ionic conductivity of reduced $La_{0.2}Sr_{0.8}Ti_{1-x}Sc_xO_3$ (x=0, 0.05, 0.1 and 0.15) on temperature. As shown in Fig 6 (a), the conductivity of the reduced $La_{0.2}Sr_{0.8}Ti_{1-x}Sc_xO_3$ (x=0, 0.05, 0.1 and 0.15) samples displays typical metallic behaviors in 5%H_2/Ar atmosphere with negative temperature coefficients, firmly confirming the metallic conductivity of the reduced $La_{0.2}Sr_{0.8}Ti_{1-x}Sc_xO_3$ samples. The reduced LSTO sample without Sc doping displays the highest conductivity at approximately 18 $S\cdot cm^{-1}$ at 800 ºC. With the increase of Sc compositions, the conductivity gradually decreases and finally drops to 4 $S\cdot cm^{-1}$ with the maximum Sc content of x=0.15 in the reduced atmosphere at 800 ºC. As stated above, the increase of Sc doping content causes the decreased concentration of Ti^{3+} as illustrated in TGA, which therefore gradually reduces the concentration of charge carrier and hence the electrical conductivity of $La_{0.2}Sr_{0.8}Ti_{1-x}Sc_xO_3$ (x=0, 0.05, 0.1 and 0.15) decreases.[30,31] With the creation of the oxygen vacancy in titanate, the ionic conductivity of Sc-doped titanate is expected to be improved. Fig. 6 (b) shows the temperature dependence of ionic conductivity of the reduced $La_{0.2}Sr_{0.8}Ti_{1-x}Sc_xO_3$ (x=0, 0.05, 0.1 and 0.15) in 5%H_2/Ar from 400 to 800 ºC, respectively. The ionic conductivities remarkably improve with temperature and finally reach 1.9×10^{-4}, 3.9×10^{-4}, 1.2×10^{-3} and 3.1×10^{-3} $S\cdot cm^{-1}$ for the reduced LSTO, $LSTS_{0.05}O$, $LSTS_{0.1}O$ and $LSTS_{0.15}O$ at 800 ºC, respectively. The ionic conductivity of $LSTS_{0.15}O$ is improved by 1 order of magnitude compared to the bare LSTO at intermediate temperatures due to the creation of sufficient oxygen vacancy in bulk by doping Sc in B-site. On the other hand, the Sc in B-site is expected to lower the oxygen migration energy as reported by R.A. Davies and P.J. Wilde.[45,46]

Fig.7 shows the AC impedance of symmetric cells based on $LSTS_xO$ (x=0, 0.05, 0.1 and 0.15) under a series of hydrogen partial pressures (pH_2 =10, 20, 40, 60, 80 and 100%). There are two intercepts with real axis in the impedance spectra in which the series resistance (R_s) corresponds to the first intercept and the electrode polarization resistance (R_p) is measured by the different between the two intercepts. The R_s and R_p is calculated using Zview software.[11] The ionic resistance of the YSZ electrolyte mainly contributes to the R_s, which generally keeps stable in a wide range of hydrogen partial pressures. However, as shown in Fig. 7 (a1) and (a2), the R_p of symmetric cell based on LSTO decreases from 6.3 to 2.2 $\Omega\cdot cm^2$ with the hydrogen partial pressure ranging from 10 to 100%, suggesting that stronger reducing atmosphere is beneficial to improvement of LSTO electrode polarization. In contrast, the R_p of symmetric cells based on $LSTS_{0.05}O$, $LSTS_{0.1}O$ and $LSTS_{0.15}O$ composite electrodes decreases from 3.6 to 1.56 $\Omega\cdot cm^2$, 3.1 to 1.42 $\Omega\cdot cm^2$ and 2.5 to 1.2 $\Omega\cdot cm^2$ as shown in Fig. 7 (b1 and b2), (c1 and c2) and (d1 and d2), respectively. This is probably due to the improved electrocatalytic activity of composite electrodes with Sc doping. On the other hand, doping with Sc increases the concentration of oxygen vacancy and accordingly leads to the enhanced ionic conductivity. Similar behaviors have also been observed for symmetric cells with LSTO, $LSTS_{0.05}O$, $LSTS_{0.1}O$ and $LSTS_{0.15}O$ composite electrode with different carbon monoxide partial pressure (pCO) ranging from 1% to 4% as in Fig.8. The R_p based on LSTO, $LSTS_{0.05}O$, $LSTS_{0.1}O$ and $LSTS_{0.15}O$ decreases from 22.7 to 7.44 Ω cm^2, 18.8 to 4.3 Ω cm^2, 15.2 to 4.8 Ω cm^2 and 12.8 to 4.1 Ω cm^2 as shown in Fig.8 (a), (b),

(c) and (d), respectively. This further demonstrates that a stronger reducing atmosphere with higher content of carbon monoxide is favorable for improved electrode performances. This redox-stable electrode shows promising polarizations even in a less reducing atmosphere with small concentration of carbon monoxide.

Fig.9 shows the microstructure of a single electrolyser with the configuration of (cathode) LSTSO-SDC/YSZ/LSM-SDC (anode). It can be found that the two electrode layers about 10 μm in thickness are porous and adhere well to the YSZ electrolyte. The direct electrolysis of pure carbon dioxide is then performed in the solid oxide electrolysers based on LSTO and $LSTS_{0.15}O$ cathodes under applied voltages ranging from 0 to 2.0 V at 800 ºC, respectively. In order to check the sealing of solid oxide electrolyser, the open circuit voltage (OCV) is recorded with the cathode and anode exposed to $5\%H_2$/Ar and static air, respectively. The OCVs reach about 1.0 V for the cells, which indicates a good separation between the anodic and cathodic gas. As shown in Fig. 10 (a), the typical curves of the current density *versus* voltage (I-V curves) are displayed for direct carbon dioxide electrolysis at 800 ºC. The change in the slope of I-V curves at approximately 1.0 V indicates two different main cell processes: (a) the electrochemical reduction of the cathodes and oxidation of the anodes at low voltage; (b) the carbon dioxide electrolysis at high voltage. The maximum current density reaches 0.21 $A \cdot cm^{-2}$ at 2.0 V with the cell based on bare LSTO cathode. In contrast, the cell based on $LSTS_{0.15}O$ cathode is largely improved and the current finally reaches approximately 0.31 $A \cdot cm^{-2}$ which improves by approximately 50% compared with LSTO electrode under the same condition. The current density with $LSTS_{0.15}O$ electrode increase steeply compared to LSTO electrode, which indicates that the $LSTS_{0.15}O$ electrode significantly enhances electrolysis performances. In order to study the resistance change of the electrolysers, dV/dI curve (total cell resistance) is plotted *versus* applied voltage as shown in Fig 10 (b). At low voltage, electrode polarisation occupies the large part of the total resistance; however, ohmic polarisation coming from ionic transportation in electrolyte gradually becomes the dominant influence under high applied potential, which implies that the ionic transport process is the main limitation at high applied voltage.

For further study of the change in R_s and R_p, the *in-situ* AC impedance spectroscopy is conducted under a series of applied voltages ranging from 1.0 to 2.0 V for the electrolysers based on LSTO and $LSTS_{0.15}O$ cathodes in Fig. 11, respectively. It is observed that the R_s values are stabilized at approximately 2.1 $\Omega \cdot cm^2$; however, the R_p values significantly improve with applied voltages from 1.0 to 2.0 V. This is because that the increasing voltage activates the electrodes and improves the electrocatalytic activity of the composite electrode. Two semicircles are observed on the impedance spectra: the high-frequency arcs (R_1) and low-frequency arcs (R_2). At high frequency, R_1 of the solid oxide electrolyzer with cathode based on bare LSTO is stable at approximately 0.7 $\Omega \cdot cm^2$ or improving in a narrow range in a wide voltage range. In contrast, the R_1 for the electrolyser with $LSTS_{0.15}O$ composite cathode is greatly decreased to approximately 0.3 $\Omega \cdot cm^2$ and further enhanced under high applied voltage. The R_1 is an indication of charge transfer and the Sc-doped cathode with improved R_1 firmly shows that the increased oxide-ion conductivity by doping with Sc greatly benefits the charge transfer and accordingly reduces the high-frequency polarization resistance. At low frequency, it is observed that the mass transfer, R_2, dominates the electrode process of the electrolyser, which is due to the dissociative adsorption, gas conversion and species transfer at three-phase boundary. The R_2 considerably improves from 4 to 1.4 $\Omega \cdot cm^2$ for the electrolyzer based on LSTO cathode with the applied voltage ranging from 1.0 to 2.0 V, indicating the improved kinetics of gas

conversion at high voltage. In contrast, the R_2 is significantly decreased to 2 $\Omega \cdot cm^2$ at low voltage and further reduced to 0.8 $\Omega \cdot cm^2$ at high voltage with the Sc-doped cathode, suggesting the greatly improved mass transfer because of the remarkable chemical adsorption of CO_2 in cathode. To further investigate the electrolysis performance of the electrolyzer with LSTO and $LSTS_{0.15}O$, both cells are performed with the cathodes fed in pure CO_2 at 800 ºC as shown in Fig. 12. The current density with Sc-doped cathode reaches approximately 0.1, 0.2 and 0.3 $A \cdot cm^{-2}$ at 1.2, 1.6 and 2.0 V, respectively, which are 1.5-2 times higher than that of the electrolyzer with LSTO cathode under the same condition. Fig. 12 shows the rate of CO production and the current efficiencies of the electrolyzers with cathodes based on LSTO and $LST_{0.15}O$ for CO_2 electrolysis at different applied voltages. Fig. 13 (a) shows the rate of CO production and the current efficiency of electrolyzers based on LSTO and LSTSO for CO_2 electrolysis at different applied voltages and the maximum CO production for the cell based on Sc-doped electrode is 1.8 $ml \cdot min^{-1} \cdot cm^{-2}$, which is much higher than 0.85 $ml \cdot min^{-1} \cdot cm^{-2}$ at 2.0 V with bare LSTO electrode. As shown in Fig. 13 (b), for the bare LSTO cathode, the maximum current efficiency reaches 61% for CO_2 electrolysis at 800 °C. In contrast, the maximum current efficiency of the cell based on Sc-doped cathode is enhanced to 82% under the same condition. The current efficiency is improved by approximately 20% with the Sc-doped cathode comparing with the bare LSTO ceramic cathode. Obviously, the solid oxide electrolyzer based on Sc-doped cathode exhibits better performance. This is because that the generated oxide vacancies improve ionic conductivity and lower electrode polarization. On the other hand, the surface oxygen vacancies could accommodate and activate CO_2 molecules *via* strong chemical bonding between oxide ions in CO_2 and the nearest cations in LSTO. In order to validate the short-term stability of the $LSTS_{0.15}O$ composite cathode, direct carbon dioxide electrolysis is performed at a fixed voltage of 1.6 V at 800 °C for 24 h with pure CO_2 fed the cathode. As shown in Fig. 14, it reveals a slight decrease in the current density within the first few hours; however, the current density is stable (approximately 0.17 $A \cdot cm^{-2}$) on the whole, which confirms the excellent short-term stability of the Sc-doped composite cathode for direct carbon dioxide electrolysis.

Conclusions

In our work, scandium is doped into the B-site of LSTO to improve the catalytic activity for direct carbon dioxide electrolysis in an oxide-ion-conducting solid oxide electrolyser. The titanate doped with scandium remarkably improves the ionic conductivity though electronic conductivity drop is also observed. The scandium-doped titanate demonstrates excellent redox stability and significantly improves electrocatalytic activity. Electrochemical measurements of direct carbon dioxide electrolysis show that the current efficiencies based on the Sc-doped cathode are improved by approximately 20% in a wide range of applied voltages.

Acknowledgements

This work was supported by the Natural Science Foundation of China No. 21303037 and Anhui International Corporation Project No.1303063014.

Notes and references

[a] Department of Energy Materials, School of Materials Science and Engineering, Hefei University of Technology, No.193 Tunxi Road, Hefei, Anhui 230009, China.
[b] Key Laboratory of Advanced Functional Materials and Devices, Hefei University of Technology, No.193 Tunxi Road, Hefei, Anhui 230009, China.
*Corresponding: xiekui@hfut.edu.cn

† Footnotes should appear here. These might include comments relevant to but not central to the matter under discussion, limited experimental and spectral data, and crystallographic data.
Electronic Supplementary Information (ESI) available: [details of any supplementary information available should be included here]. See DOI: 10.1039/b000000x/

1 R. Lan, S.W. Tao and J.T.S. Irvine, *Energy Environ. Sci*., 2010, **3**, 438-441.

2 X.D. Yang and J.T.S. Irvine, *J. Mater. Chem*., 2008, **18**, 2349-2354.

3 K. Xie, Y.Q. Zhang, G.Y. Meng and J.T.S. Irvine, *J. Mater. Chem*., 2011, **21**, 195-198.

4 S.D. Ebbesen, R. Knibbe and M. Mogensen, *J. Electrochem. Soc*., 2012, **159**, F482-F489.

5 Y.X. Li, J. Zhou, D.H. Dong, Y. Wang, J.Z. Jiang, H.F. Xiang and X. Kui, *Phys. Chem. Chem. Phys*., 2012, **14**, 15547-15553.

6 M.A. Laguna-Bercero, J.A. Kilner and S. J. Skinner, *Chem. Mater*., 2010, **22**, 1134-1141.

7 S.D. Ebbesen and M. Mogensen, *J. Power Sources*, 2009, **193**, 349-358.

8 G. Tsekouras, D. Neagu and J.T.S. Irvine, *Energy Environ. Sci*., 2013, **6**, 256-266.

9 G.J. Wu, K. Xie, Y.C. Wu, W.T. Yao and J.N. Zhou, *J. Power Sources*, 2013, **232**, 187-192.

10 S.W. Tao and J.T.S. Irvine, *Nat. Mater*., 2003, **2**, 320-323.

11 Y.X. Li, Y. Gan, Y. Wang, K. Xie and Y.C. Wu, *Int. J. Hydrogen Energy*, 2013, **38**, 10196-10207.

12 V.B. Vert, F.V. Melo, L. Navarrete and J.M. Serra, *Appl. Catal. B Environ*., 2012, **115-116**, 346-356.

13 N. Danilovic, A. Vincent, J.L. Luo, K.T. Chuang, R. Hui and A.R. Sanger, *Chem. Mater*., 2010, **22**, 957-965.

14 J.C. Ruiz-Morales, J. Canales-Vázquez, C. Savaniu, D. Marrero-López, W.Z. Zhou and J.T.S. Irvine, *Nature*, 2006, **439**, 568-571.

15 F. Bidrawn, G. Kim, G. Corre, J. T. S. Irvine, J. M. Vohs and R. J. Gorte, *J. Electrochem. Soc*., 2008, **11**, B167-B170.

16 S.S. Xu, S.S. Li, W.T. Yao, D.H. Dong and K. Xie, *J. Power Sources*, 2013, **230**, 115-121.

17 S.W. Tao and J.T.S. Irvine, *Chem. Mater*., 2004, **16**, 4116-4121.

18 Y. Gan, J. Zhang, Y.X. Li, S.S. Li, K. Xie and J.T.S. Irvine, *J. Electrochem. Soc*., 2012, **159**, F763-F767.

19 A. Huber, M. Falk, M. Rohnke, B. Luerßen, L. Gregoratti, M. Amati and J. Janek, *Phys. Chem. Chem. Phys*., 2012, **14**, 751-758.

20 Q.Q. Qin, G.J. Wu, S.G. Chen, W. Doherty, K. Xie and Yucheng Wu, *Electrochim. Acta*, 2014, **127**, 215-227.

21 X. Li, H.L. Zhao, N.S. Xu, X. Zhou, C.J. Zhang and N. Chen, *Int. J. Hydrogen Energy*, 2009, **34**, 6407-6414.

22 D. Neagu and J.T.S. Irvine, *Chem. Mater*., 2010, **22**, 5042-5053.

23 S.S. Li, Y.X. Li, Y. Gan, K. Xie and G.Y. Meng, *J. Power Sources*, 2012, **218**, 244-269.

24 W.T. Qi, Y. Gan, D. Yin, Z.Y. Li, G.J. Wu, K. Xie and Y.C. Wu, *J. Mater. Chem. A*, 2014, **2**, 6904-6915.

25 D.N. Miller and J.T.S. Irvine, *J. Power Sources*, 2011, **196**, 7323-7327.

26 W.T. Qi, C. Ruan, G.J. Wu, Y. Zhang, Y. Wang, K. Xie and Y.C. Wu, *Int. J. Hydrogen Energy*, 2014, **39**, 5485-5496.

27 X.L. Yue and J.T.S. Irvine, *J. Electrochem. Soc*., 2012, **159**, F442-F448.

28 Y. Gan, Q.Q. Qin, S.G. Chen, Y. Wang, D.H. Dong, K. Xie and Y.C. Wu, *J. Power Sources*, 2014, **245**, 245-255.

29 A. Hauch, S.D. Ebbesen, S.H. Jensen and M. Mogensen, *J. Mater. Chem*., 2008, **18**, 2331-2340.

30 P.Y. Zeng, R. Ran, Z.H. Chen, W. Zhou, H.X. Gu, Z.P. Shao and S.M. Liu, *J. Alloys Compd*., 2008, **455**, 465-470.

31 X. Li, H.L. Zhao, F. Gao, N. Chen and N.S. Xu, *Electrochem. Commun*., 2008, **10**, 1567-1570.

32 J. Canales-Vázquez, J.C. Ruiz-Morales, J.T.S. Irvine and W.Z. Zhou, *J. Electrochem. Soc*., 2007, **152**, A1458-A1465.

33 X.L. Yue, A.Y. Yan, M. Zhang, L. Liu, Y.L. Dong and M.J. Cheng, *J. Power Sources*, 2008, **185**, 691-697.

34 M. Nolan, *J. Phys. Chem. C*, 2009, **113**, 2425-2432.

35 L.F. Liao, C.F. Lien, D.L. Shieh, M.T. Chen and J.L. Lin, *J. Phys. Chem. B*, 2002, **106**, 11240-11245.

36 T.L. Thompson, O. Diwald and J.T. Yates, *J. Phys. Chem. B*, 2003, **107**, 11700-11704.

37 K. Xie, Y.Q. Zhang, G.Y. Meng and J.T.S. Irvine, *Energy Environ. Sci*., 2011, **4**, 2218-2222.

38 S.S. Li, Q.Q. Qin, K. Xie, Y. Wang and Y.C. Wu, *J. Mater. Chem.A*, 2013, **1**, 8984-8993.

39 Y Matsumoto, T Shono, T Hasegawa, T Fukumura, M Kawasaki, P Ahmet, T Chikyow, S Koshihara, H Koinuma, *Science*, 2001, **291**, 854-856.

40 C.X. Wang , X.B. Chen, A.P. Zhu, *Solid State Commun*., 2012, **152**, 1067-1071.

41 R. S. Kumar, A. Z. Barasheed and H. N. Alshareef, *ACS Appl. Mater. Interfaces*, 2013, **5**, 7268-7273.

42 Badrinarayanan, S. Sinha and A. B. Mandale, *J. Electron Spectrosc*., 1989, **49**, 303-309.

43 M. S. J. Marshall, D. T. Newell, D. J. Payne, R. G. Egdell and M. R. Cast, *Phys. Rev. B*, **83**, 035410-1-035410-6.

44 M.C. Biesinger, L.W.M. Laua, A.R. Gerson and R.S.C. Smart, *Appl. Surf. Sci*., 2010, **257**, 887-898.

45 R.A. Daviesa, M.S. Islama and J.D. Galeb, *Solid State Ionics*, 1999, **126**, 323-335.

46 P.J. Wilde and C.R.A. Catlow, *Solid State Ionics*, 1998, **122**, 173-183.

Table 1 The parameters of oxidized $La_{0.2}Sr_{0.8}Ti_{1-x}Sc_xO_{3+\delta}$ (x=0, 0.05, 0.1 and 0.15).

x	Crystal system	Crystal space	a=b=c(Å)	α=β=γ (°)	Volume (Å^3)
0	Cubic	Pm-3m	3.9047(4)	90	59.536
0.05			3.9068(3)		59.723
0.1			3.9095(5)		59.756
0.15			3.9122(6)		59.881

Table 2 The parameters of reduced $La_{0.2}Sr_{0.8}Ti_{1-x}Sc_xO_{3+\delta}$ (x=0, 0.05, 0.1 and 0.15).

x	Crystal system	Crystal space	a=b=c(Å)	α=β=γ (°)	Volume (Å^3)
0	Cubic	Pm-3m	3.9082(4)	90	59.696
0.05			3.9090(1)		59.731
0.1			3.9112(3)		59.833
0.15			3.9131(9)		59.957

Fig 1: XRD of the oxidized $La_{0.2}Sr_{0.8}Ti_{1-x}Sc_xO_{3+\delta}$ (x=0, 0.05, 0.1, 0.15 and 0.2) (a) and the reduced $La_{0.2}Sr_{0.8}Ti_{1-x}Sc_xO_3$ (x=0, 0.05, 0.1 and 0.15) (b), cell parameters of oxidized (c) and reduced (d) $La_{0.2}Sr_{0.8}Ti_{1-x}Sc_xO_3$ (x=0, 0.05, 0.1 and 0.15).

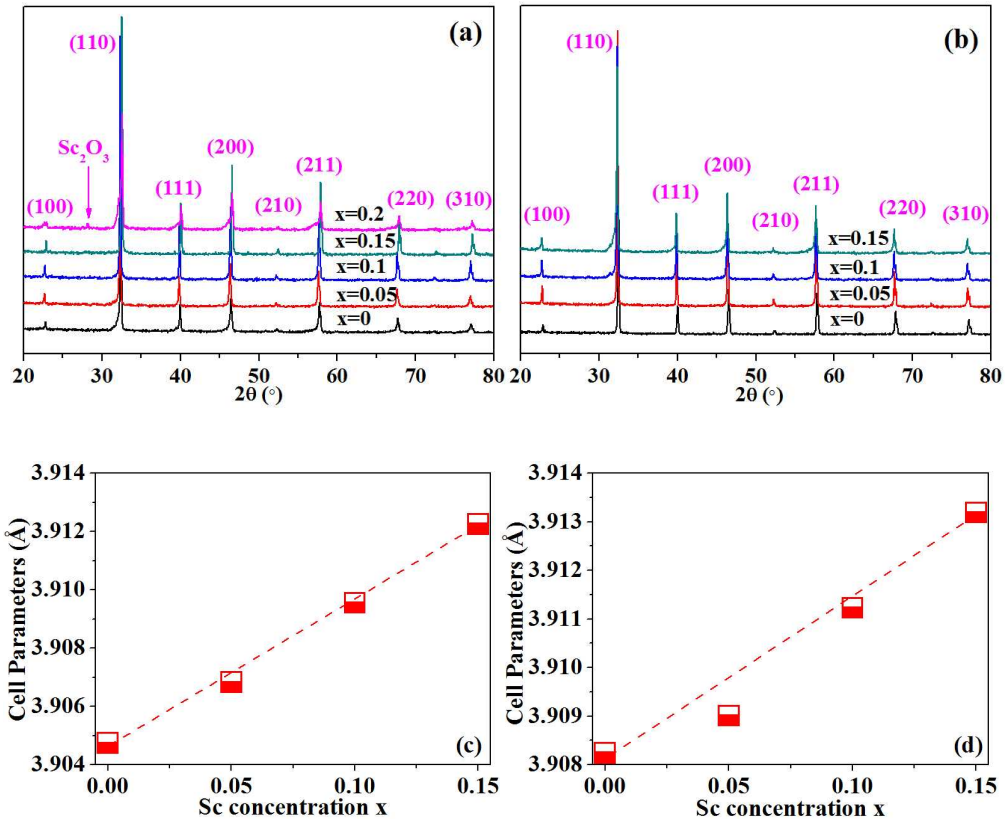

Fig 2: XRD rietveld refinement patterns of oxidized and reduced LSTO (a1 and a2) and oxidized $LSTS_{0.15}O$ (b1 and b2).

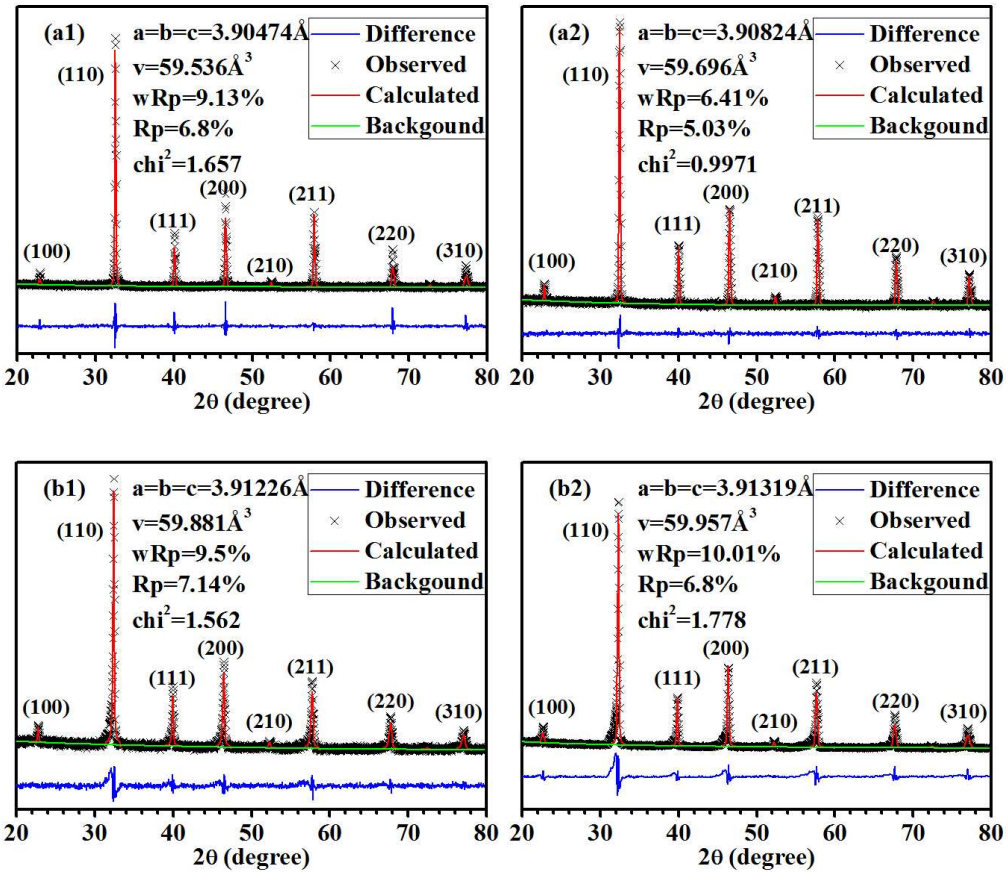

Fig 3: TEM results of oxidized of LSTO (a1), reduced LSTO (a1), oxidized $LSTS_{0.15}O$ (b1) and oxidized $LSTS_{0.15}O$ (b2).

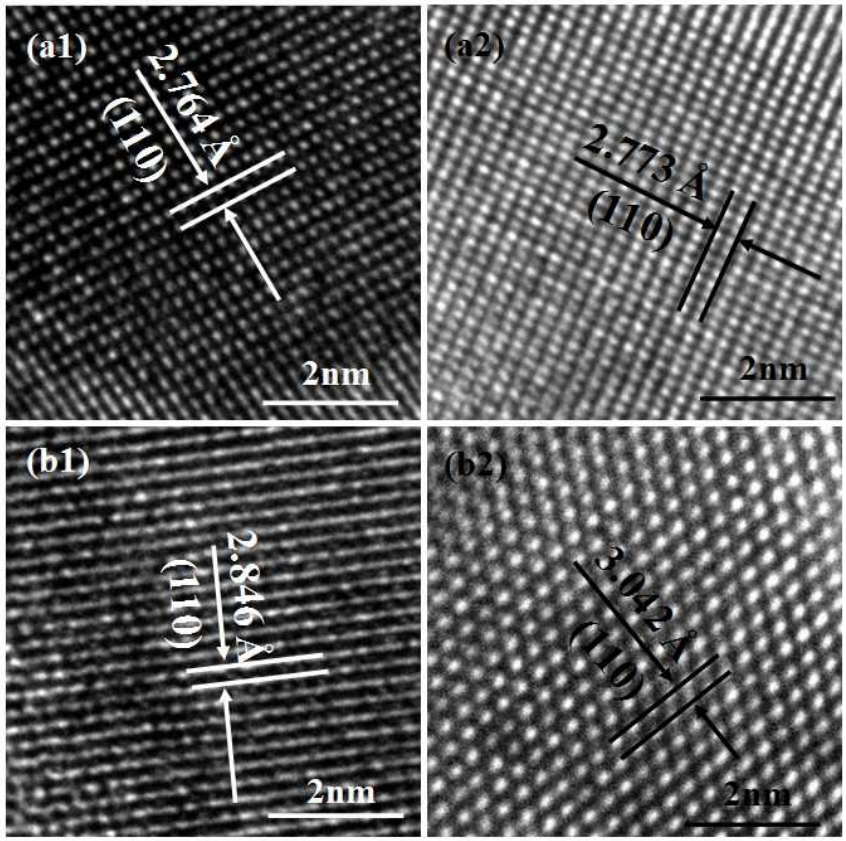

Fig 4: XPS results of (a1) Ti and in (a2) Sc oxidized $La_{0.2}Sr_{0.8}Ti_{0.85}Sc_{0.15}O_3$ ($LSTS_{0.15}O$); (b1) Ti and (b2) Sc in reduced $La_{0.2}Sr_{0.8}Ti_{0.85}Sc_{0.15}O_3$ ($LSTS_{0.15}O$).

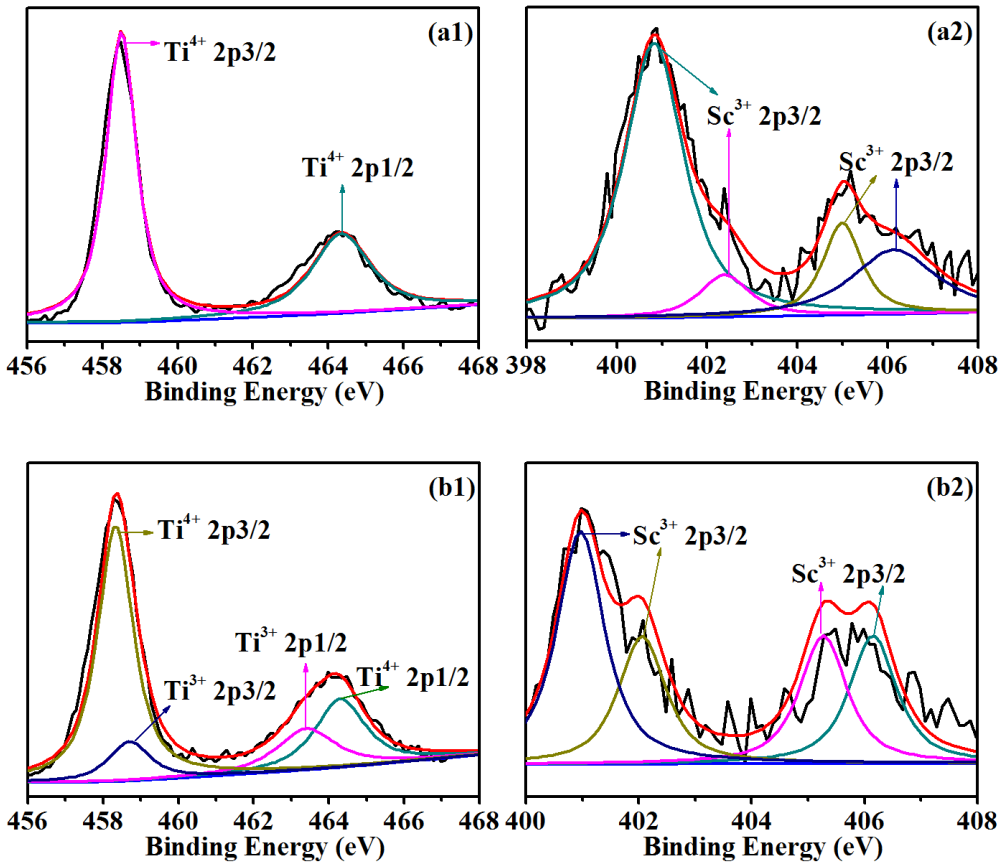

Fig 5: TGA and DSC results of oxidized LSTO (a) and oxidized $LSTS_{0.15}O$ (b) from room temperature to 1000 ºC.

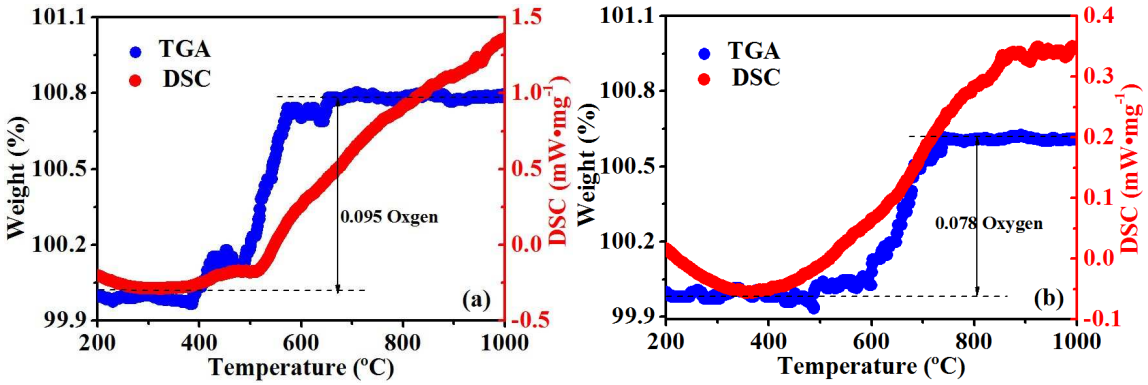

Fig 6: (a) the conductivity of reduced $La_{0.2}Sr_{0.8}Ti_{1-x}Sc_xO_3$ (x=0, 0.05, 0.1 and 0.15) *versus* temperature from 300 to 800 °C; (b) the ion conductivity of reduced $La_{0.2}Sr_{0.8}Ti_{1-x}Sc_xO_3$ (x=0, 0.05, 0.1 and 0.15) *versus* temperature from 400 to 800 ºC.

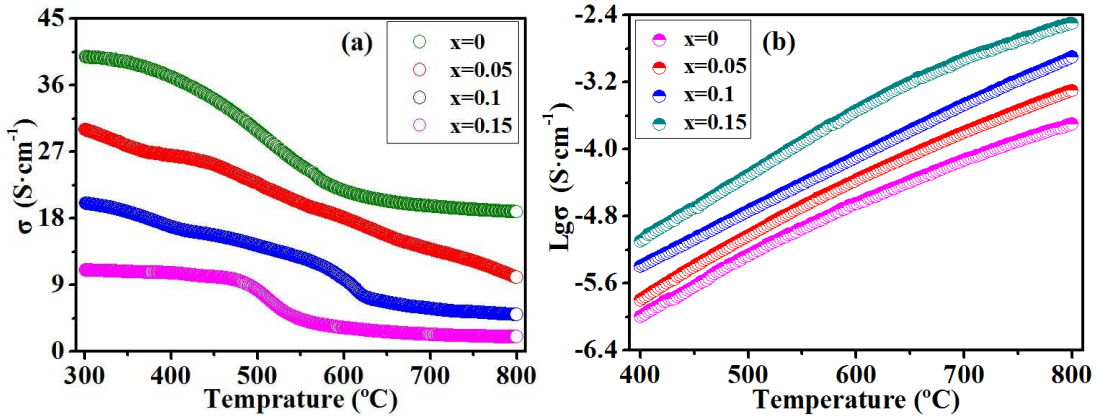

Fig 7: AC impedance spectroscopy of the symmetric cells with the configurations $LSTS_xO$-SDC /YSZ/$LSTS_xO$-SDC (x=0) (a1 and a2), (x=0.05) (b1 and b2), (x=0.1) (c1 and c2) and (x=0.15) (d1 and d2) tested under different hydrogen partial at 800 ºC.

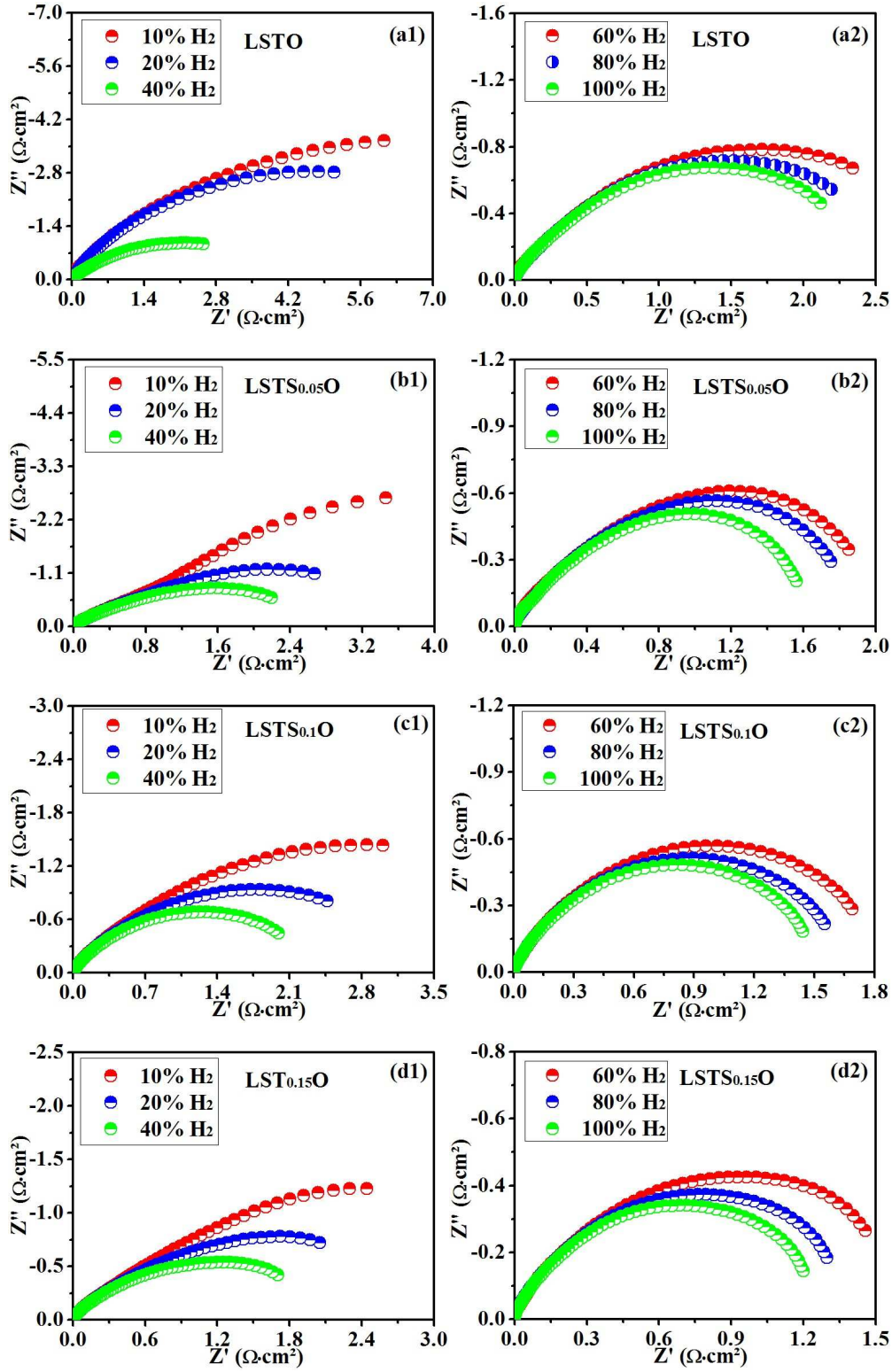

Fig 8: AC impedance spectroscopy of the symmetric cells with the configurations $LSTS_xO$-SDC /YSZ/$LSTS_xO$-SDC (x=0) (a), (x=0.05) (b), (x=0.1) (c) and (x=0.15) (d) tested under different carbon monoxide partial at 800 ºC.

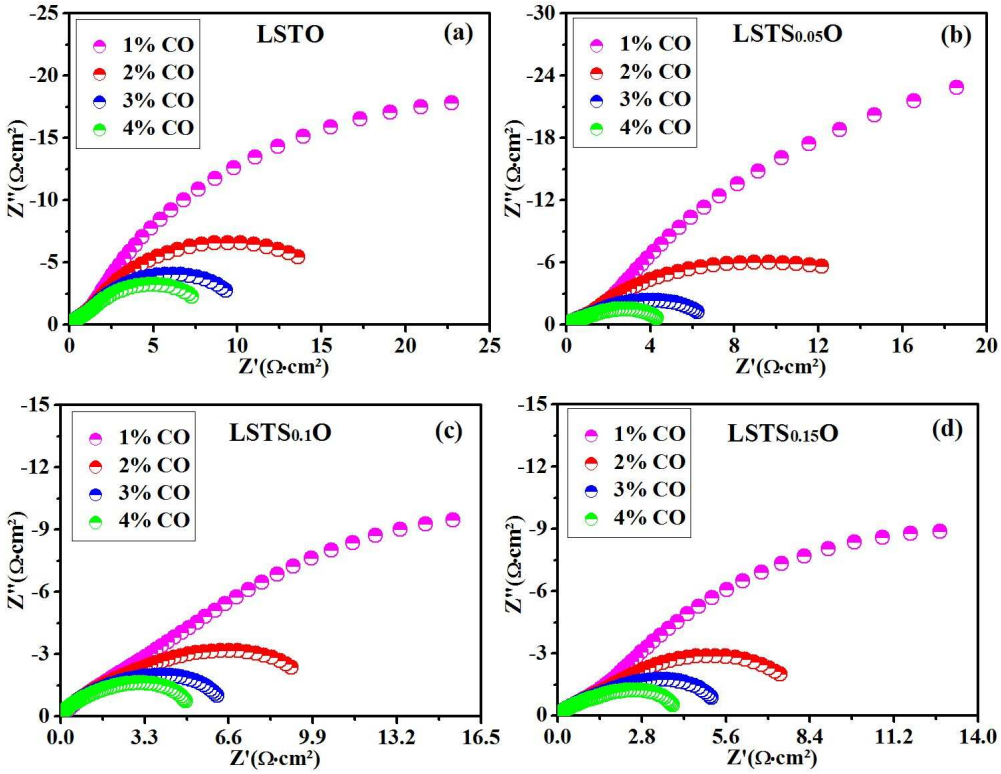

Fig 9: The cross-sectional views of the solid oxide electrolyzer based on LSTSO-SDC cathode and LSM-SDC anode.

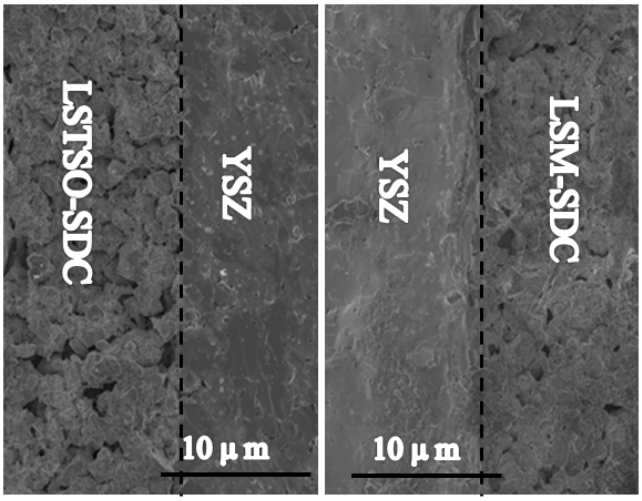

Fig 10: I-V curves of Single electrolyzers with cathodes based on LSTO-SDC and $LSTS_{0.15}O$-SDC cathode for CO_2 electrolysis; the dV/dI curve of the electrolyzers based on LSTO-SDC and $LSTS_{0.15}O$-SDC cathode.

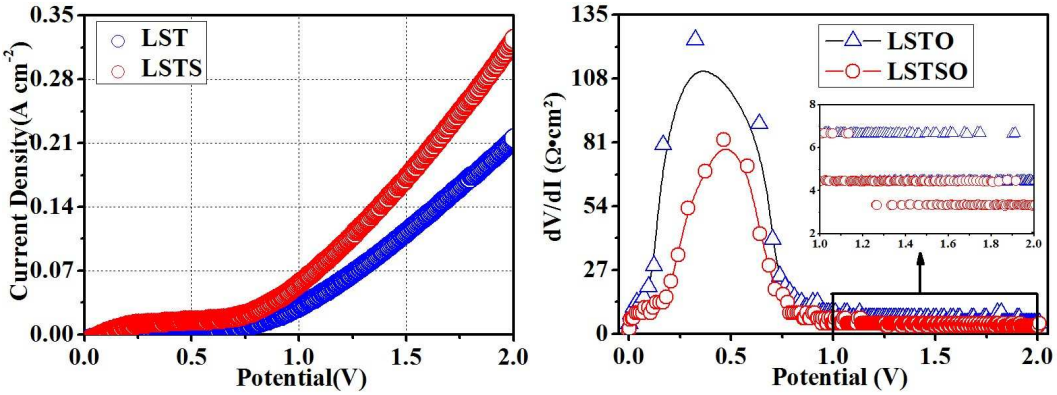

Fig 11: AC impedance of single electrolyzers with cathodes based on (a1and a2) LSTO-SDC and (b1 and b2) $LSTS_{0.15}O$-SDC under different applied potentials with the flow of CO_2 at 800 ºC.

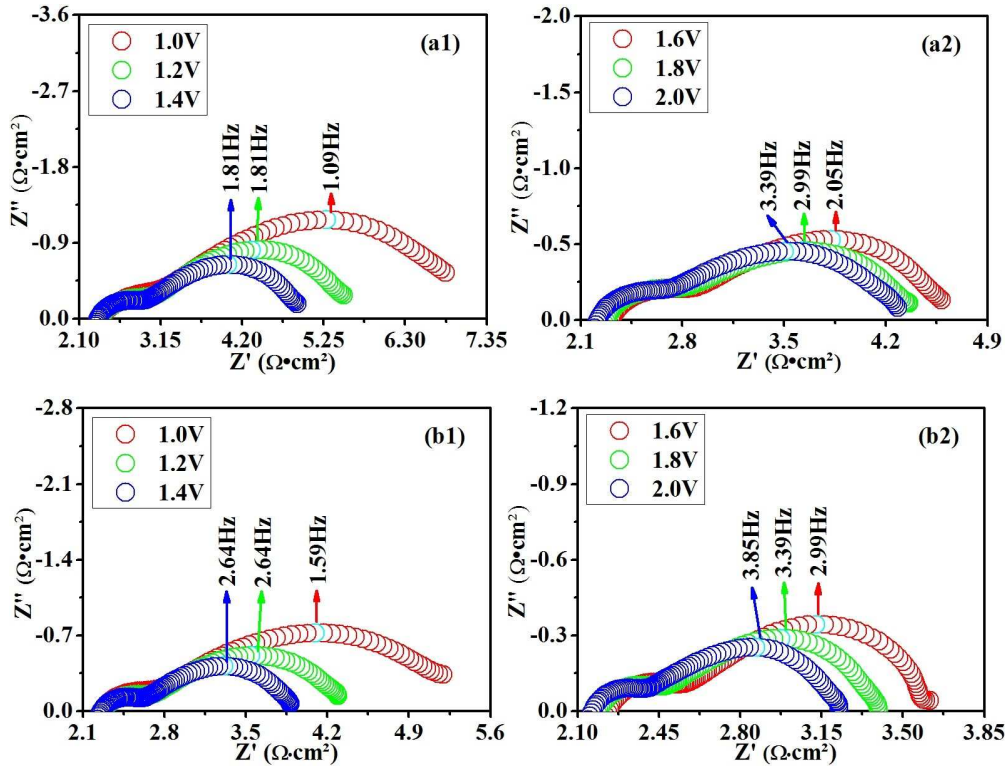

Fig 12: The performance of single electrolyzers with cathodes based on (a) LSTO-SDC and (b) $LSTS_{0.15}O$-SDC under different applied potentials at 800 ºC for CO_2 electrolysis.

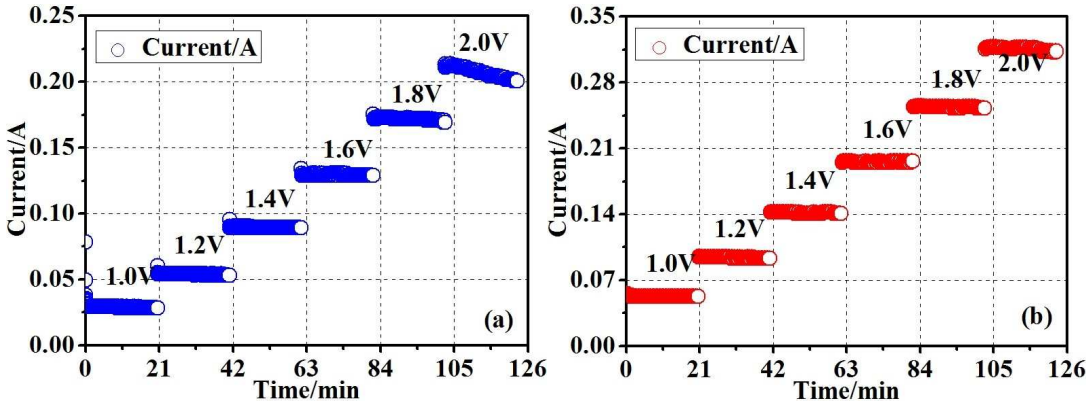

Fig 13: (a) the production of CO and (b) the corresponding Faraday efficiency for CO_2 electrolysis under different applied potentials.

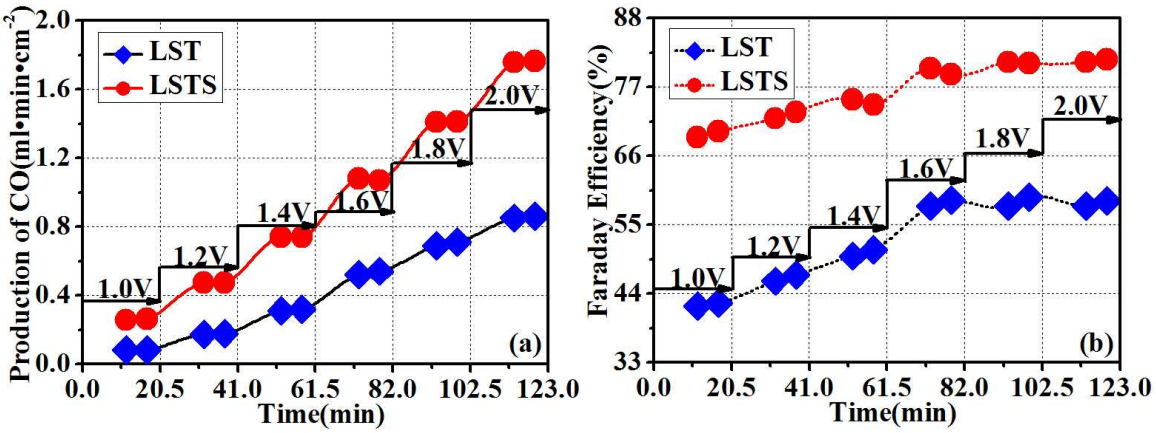

Fig 14: Short-term performance of single electrolyzer based on $LSTS_{0.15}O$-SDC cathode with the flow of CO_2 at 1.6 V at 800 °C.